Nuclear Instruments and Methods in Physics Research B 100 (1995) 31-46

NIM B
Beam Interactions with Materials & Atoms

ELSEVIER

PENELOPE: An algorithm for Monte Carlo simulation of the penetration and energy loss of electrons and positrons in matter

J. Baró [a], J. Sempau [b], J.M. Fernández-Varea [c], F. Salvat [c,*]

[a] *Serveis Científico-Tècnics, Universitat de Barcelona, Martí i Franqués s/n, 08028 Barcelona, Spain*
[b] *Institut de Tècniques Energètiques, Universitat Politècnica de Catalunya, Diagonal 647 bis, 08028 Barcelona, Spain*
[c] *Facultat de Física (ECM), Universitat de Barcelona, Societat Catalana de Física (IEC), Diagonal 647, 08028 Barcelona, Spain*

Received 30 September 1994

Abstract

A mixed algorithm for Monte Carlo simulation of relativistic electron and positron transport in matter is described. Cross sections for the different interaction mechanisms are approximated by expressions that permit the generation of random tracks by using purely analytical methods. Hard elastic collisions, with scattering angle greater than a preselected cutoff value, and hard inelastic collisions and radiative events, with energy loss larger than given cutoff values, are simulated in detail. Soft interactions, with scattering angle or energy loss less than the corresponding cutoffs, are simulated by means of multiple scattering approaches. This algorithm handles lateral displacements correctly and completely avoids difficulties related with interface crossing. The simulation is shown to be stable under variations of the adopted cutoffs; these can be made quite large, thus speeding up the simulation considerably, without altering the results. The reliability of the algorithm is demonstrated through a comparison of simulation results with experimental data. Good agreement is found for electrons and positrons with kinetic energies down to a few keV.

1. Introduction

The problem of the penetration and energy loss of fast electrons in matter has attracted great attention since the beginning of this century. Since most of our knowledge about nuclear, atomic, molecular and solid state structure has been, and is being, achieved by using electron beams to probe matter, this problem is of fundamental interest. A detailed description of electron, and positron, transport is required in a number of fields such as beta-ray spectrometry [1,2], electron microscopy [3] and electron and positron surface spectroscopy [4,5]. Accurate information on high energy electron and positron transport is also needed in radiation dosimetry and radiotherapy [6].

Electron multiple scattering processes were first treated on the basis of the transport theory [7,8]. Since the beginning of the sixties, with the increasing availability of fast computers, Monte Carlo (MC) simulation methods have been developed and applied to many experimental situations (see e.g. Ref. [9]). The characteristics of different MC simulation schemes depend mainly on the energy range of interest. "Detailed" MC simulation [10,11] where *all* scattering events experienced by an electron are described in chronological succession, is feasible at low energies. Detailed simulation is virtually exact, i.e. simulation results are identical to those obtained from the exact solution of the transport equation with the same scattering model (except for statistical uncertainties). For progressively higher energies, however, the average number of scattering events per track increases gradually and eventually detailed simulation becomes unfeasible.

For high energies, most of the MC codes currently available (e.g. ETRAN [9], EGS4 [12], GEANT [13]) have recourse to multiple scattering theories which allow the simulation of the global effect of a large number of events in a track segment of a given length (step). Following Berger [14], these simulation procedures will be referred to as "condensed" MC methods. The multiple scattering theories implemented in condensed simulation algorithms are only approximate and lead to systematic errors, which arise mainly from the lack of knowledge about the spatial distribution of the particle after travelling a given path length. These errors can be made evident by the dependence of the simulation results on the adopted step length [9]. To analyze their magnitude, one can perform simulations of the same experimental arrangement with different step lengths. Usually, it is found that the results stabilize when reducing the step length, but the computation time increases rapidly, roughly in proportion to the inverse of the step length. Thus,

* Corresponding author. Tel. +34 3 402 1186, fax +34 3 4021174, e-mail: cesc@ecm.ub.es

SSDI 0168-583X(95)00349-5

for each particular problem, one must reach a compromise between available computer time and attainable accuracy. It is also worth noting that, owing to the nature of certain multiple scattering theories and/or to the particular way they are implemented in the simulation code, the use of very short step lengths may introduce artifacts in the simulation results. For instance, the multiple elastic scattering theory of Molière [15], which is the one used in EGS4 based codes, is not applicable to step lengths shorter than a few times the elastic mean free path [16,17] and multiple elastic scattering has to be switched off when the step length becomes smaller than this value [18]. Evidently, stabilization for short step lengths does not necessarily imply that simulation results are correct. Condensed schemes also have difficulties to properly handle particle tracks in the vicinity of an interface, i.e. a surface separating two media of different compositions [18].

A third class of simulation schemes, the so-called "mixed" simulation methods [14,19,20], combines detailed simulation of hard events, i.e. events with polar scattering angle θ or energy loss W larger than previously selected cutoff values θ_S and W_c, with condensed simulation of soft interactions with $\theta < \theta_S$ or $W < W_c$. Owing to the fact that, for high-energy electrons, the differential cross sections (DCS) for the various interaction processes decrease rapidly when θ or W increase, cutoffs can be selected such that the mean number of hard events per track is sufficiently small to allow their detailed simulation (i.e. a few hundred at most). Hard events cause large angular deflections and energy losses, which can only be properly reproduced through detailed simulation. On the other hand, soft interactions have a mild effect on the evolution of the track, which can be accurately simulated by using a multiple scattering approach. Mixed simulation is preferable to condensed simulation because i) spatial distributions are more correctly simulated, ii) tracks in the vicinity of interfaces are properly handled, and iii) possible dependencies of the results on user-defined parameters are largely reduced.

In this paper we describe a mixed simulation algorithm called PENELOPE (an acronym that stands for PENetration and Energy LOss of Positrons and Electrons). The adopted single scattering DCSs for inelastic collisions and bremsstrahlung emission have been described by Salvat and Fernández-Varea [21]. Approximate simulation methods for elastic scattering have been considered in previous works [16,22]; here we adopt the W2D model introduced in Ref. [22].

In Section 2 we consider various aspects of the adopted single scattering DCSs and pertinent sampling techniques not covered in Refs. [21] and [22]. Mixed simulation strategies to speed up the simulation of high-energy particles are presented in Section 3. The complete simulation algorithm is described in Section 4. Section 5 contains an analysis of the stability of the simulation results under changes in the adopted cutoff values of the angular deflection and the energy loss. Finally, the reliability of this simulation scheme is demonstrated by comparing simulation results and experimental data.

2. Single scattering model

Let us consider a fast particle, electron or positron, with kinetic energy E moving in a single-element medium of atomic number Z. The extension to compounds and mixtures will be treated below. The number of atoms per unit volume is given by

$$N = \frac{N_A \rho}{A_w}, \tag{1}$$

where N_A is the Avogadro number, ρ is the mass density of the material and A_w is the atomic weight.

The possible interactions of the particle with the medium are elastic scattering, inelastic collisions and bremsstrahlung emission (and annihilation in the case of positrons). Each kind of interaction is characterized by a single scattering atomic DCS, which determines the associated mean free path and the probability density functions of the scattering angle θ and the energy loss W in each individual interaction. The DCSs adopted in PENELOPE are sufficiently accurate for most practical simulation purposes and permit the random sampling of the scattering angle and the energy loss completely analytically, so that sampling errors that could originate from numerical interpolation are readily avoided. It is worth pointing out that *multiple* scattering distributions are quite insensitive to the fine details of the single scattering DCSs. If the adopted DCSs have a physically reasonable shape, only a few quantities, obtained by integrating the DCS over θ or W, have a direct influence on the simulation results [16,23]. As a consequence, a general purpose simulation procedure can be made much simpler by using analytical approximate DCSs leading to the correct values of these relevant integrals.

The transport of photons is not included in the present simulations. A code for the simulation of electron-photon showers, which combines PENELOPE with a conventional procedure to follow photon histories [24], is currently being checked and will be described elsewhere.

2.1. Elastic scattering

Single elastic collisions are determined by the values of the polar and azimuthal scattering angles, θ and ϕ respectively. Assuming that the scattering potential has spherical symmetry, single and multiple scattering angular distributions are axially symmetrical about the direction of incidence, i.e. they are independent of the azimuthal scattering angle ϕ. For our purposes, it is convenient to measure angular deflections produced by single scattering events in terms of the variable

$$\mu \equiv \frac{1 - \cos\theta}{2} \tag{2}$$

instead of the scattering angle θ.

Let $d\sigma_{el}/d\mu$ denote the single scattering DCS. The mean free path λ_{el} between elastic events is given by

$$\lambda_{el}^{-1} = N\sigma_{el} = N\int_0^1 \frac{d\sigma_{el}}{d\mu}\, d\mu, \tag{3}$$

where σ_{el} is the total elastic cross section. The first and second transport mean free paths, λ_1 and λ_2, are defined by (see Ref. [16])

$$\lambda_1^{-1} = N\int_0^1 2\mu\frac{d\sigma_{el}}{d\mu}\, d\mu \tag{4}$$

and

$$\lambda_2^{-1} = N\int_0^1 6(\mu-\mu^2)\frac{d\sigma_{el}}{d\mu}\, d\mu. \tag{5}$$

We consider that accurate values of the mean free path, λ_{el}, and transport mean free paths λ_1 and λ_2 are known. These can be directly obtained from partial wave calculations for low energies, and from suitable approximations for high energies. In the simulations reported below, for electrons and positrons with kinetic energies less than 1.5 MeV, we have adopted the values of these quantities obtained from partial wave calculations, using the PWADIR code described in Ref. [25] with the analytical Dirac–Hartree–Fock–Slater atomic scattering potential [26] (including solid-state effects, and exchange effects in the case of electrons). For higher energies, transport mean free paths have been calculated from the screened Mott formula described in Ref. [27]. This formula is not accurate for very small scattering angles; hence, a different approach should be used to obtain the mean free path or, equivalently, the total elastic cross section σ_{el}, which strongly depends on the small-angle behaviour of the DCS. The total cross section for $E > 1.5$ MeV has been computed from the optical theorem, using the forward scattering amplitude for the free atom analytical Dirac–Hartree–Fock–Slater potential obtained from the eikonal approximation [28]. The mean free paths and transport mean free paths used in the simulations are expected to be reliable for energies from ~ 1 keV up to several hundred MeV. These quantities are tabulated for a grid of kinetic energies, and transformed into continuous functions of the energy by means of cubic spline interpolation on a log-log scale.

Elastic scattering is simulated here by using the W2D model described in Ref. [22]. Essentially, this is a model DCS which yields multiple scattering distributions that do not differ significantly from those obtained from the actual scattering process. The W2D single scattering DCS is given by (cf. Eq. (3))

$$\frac{d\sigma_{el}^{(W2D)}}{d\mu} = \frac{1}{N\lambda_{el}}p_{ap}(\mu), \tag{6}$$

where λ_{el} is the tabulated mean free path and

$$p_{ap}(\mu) \equiv (1-B)\frac{A(1+A)}{(\mu+A)^2} + B\delta(\mu-\mu_0). \tag{7}$$

The parameters A (> 0), B ($0 \le B < 1$) and μ_0 ($0 \le \mu_0 \le 1$) are determined in such a way that the mean and variance of the approximate distribution $p_{ap}(\mu)$ are the same as those obtained from the actual DCS or, equivalently,

$$\int_0^1 \mu p_{ap}(\mu)\, d\mu = \frac{1}{2}\frac{\lambda_{el}}{\lambda_1} \tag{8}$$

and

$$\int_0^1 \mu^2 p_{ap}(\mu)\, d\mu = \frac{1}{2}\frac{\lambda_{el}}{\lambda_1} - \frac{1}{6}\frac{\lambda_{el}}{\lambda_2}. \tag{9}$$

Thus, the average path length between collisions and the mean and variance of the angular deflection μ in each elastic collision obtained from the W2D model are identical to the values obtained from the actual DCS (i.e. the DCS calculated as described above). A detailed analysis of the reliability of the W2D model has been presented in Ref. [22], where explicit analytical formulas for random sampling of the angular deflection μ in single elastic events are given. Notice that the model parameters are completely determined by the quantities λ_{el}, λ_1 and λ_2. In principle, it can be applied to any scattering law.

2.2. Inelastic collisions

Inelastic collisions of electrons and positrons in dense media are simulated in terms of the analytical DCSs described in Ref. [21]. The basis of this treatment is a generalized oscillator strength model where each electron shell is replaced by a single oscillator with strength f_i equal to the number of electrons in the shell and resonance energy $W_i = aU_i$, where U_i is the ionization energy of the shell [29]. Excitations of the conduction band are accounted for by a single oscillator with oscillator strength f_{cb} and resonance energy W_{cb} ($U_{cb} = 0$). The semi-empirical adjustment factor a is introduced to obtain agreement with the adopted mean excitation energy I, which is taken from Ref. [30]. Its numerical value is given by

$$\ln a = (Z - f_{cb})^{-1}\left[Z\ln I - f_{cb}\ln W_{cb} - \sum f_i \ln U_i\right]. \tag{10}$$

The DCS for inelastic scattering is a function of the energy loss W and the polar scattering angle θ of the projectile.

Instead of the scattering angle, it is customary to use the recoil energy Q defined by

$$Q(Q+2mc^2) = c^2(p^2 + p'^2 - 2pp'\cos\theta), \tag{11}$$

where m is the electron mass, c is the velocity of light and p and p' are the magnitudes of the momentum of the projectile before and after the collision. These latter quantities are given by

$$(cp)^2 = E(E+2mc^2)$$
$$\text{and} \tag{12}$$
$$(cp')^2 = (E-W)(E-W+2mc^2).$$

The contribution to the generalized oscillator strength of a unit strength oscillator with resonance energy W_i (i.e. the excitation spectrum of this oscillator) is given by

$$F(W_i;Q,W) = \delta(W-W_i)\Theta(W_i-Q) + \delta(W-Q)\Theta(Q-W_i), \tag{13}$$

where $\delta(x)$ and $\Theta(x)$ are the Dirac delta function and the Heaviside step function, respectively. The first term in this expression corresponds to excitations with small momentum transfer, that is, distant collisions (large impact parameter) in a semiclassical picture, which have a resonant-like character ($W = W_i$). The allowed recoil energies in distant collisions lie in the interval from $Q_- = Q(\theta = 0)$ to W_i. The second term corresponds to close collisions, which are described as binary collisions with free electrons at rest ($Q = W$), by means of the Møller and Bhabha DCSs.

The energy loss DCS per atom can be written in the form

$$\frac{d\sigma_{col}}{dW} \equiv \sum_{i=1}^{M} f_i \left(\frac{d\sigma_{ci}}{dW} + \frac{d\sigma_{di}}{dW} \right), \tag{14}$$

where the summation runs over the different oscillators. The first and second terms in the parentheses stand for the partial DCSs, per unit oscillator strength, for close and distant collisions with the i-th oscillator respectively. Explicit analytical expressions for these partial DCSs are given in Ref. [21].

The generation of random values of the energy loss W and the polar scattering angle θ in single inelastic collisions is performed by using the analytical sampling methods described in Ref. [21]. It is assumed that, in collisions with the i-th oscillator, a secondary electron (delta ray) with kinetic energy $E_s = W - U_i$ ($E_s = W$ for excitations of the conduction band) is emitted in the direction of the momentum transfer.

The mean free path between inelastic collisions $\lambda_{col}(E)$, the collision stopping power $S_{col}(E)$ and the energy straggling parameter $\Omega^2_{col}(E)$ are given by

$$\lambda^{-1}_{col}(E) = N \int_0^E \frac{d\sigma_{col}}{dW}\, dW, \tag{15}$$

$$S_{col}(E) = N \int_0^E W \frac{d\sigma_{col}}{dW}\, dW \tag{16}$$

and

$$\Omega^2_{col}(E) = N \int_0^E W^2 \frac{d\sigma_{col}}{dW}\, dW. \tag{17}$$

With the adopted DCSs, all these integrals can be computed analytically. The resulting stopping powers agree closely with currently accepted values, and the mean free paths do not differ significantly from available experimental data for energies down to a few hundred eV [21]. The DCSs given by Eq. (14) should thus yield a quite accurate average description of inelastic collisions. However, the present approach is not adequate for the simulation of energy loss distributions in single or plural inelastic scattering at high energy resolution, since the energy loss spectrum at small angles (small momentum transfers) is modelled as a single resonance (δ-distribution). As a consequence, the simulated energy loss spectra show unphysical sharp peaks at energy losses that are multiples of the resonance energies. These spurious peaks are automatically smoothed out when inelastic scattering is multiple or when the bin width used to tally the energy loss distributions is larger than $\sim$100 eV (which is the order of magnitude of the difference between resonance energies of neighbouring oscillators).

2.3. Bremsstrahlung emission

The DCS per atom for bremsstrahlung emission is obtained from the corrected Bethe–Heitler formula with exponential screening derived in Ref. [21]. The DCS, differential in the energy W of the emitted photon, is

$$\frac{d\sigma_{rad}}{dW} = (E+mc^2)^{-1} \frac{d\sigma_{BHW}}{d\epsilon}, \tag{18}$$

where $d\sigma_{BHW}/d\epsilon$ is the DCS in terms of the reduced energy loss $\epsilon \equiv W/(E+mc^2)$, which is given by the analytical expression (49) in Ref. [21].

Although the mean free path for bremsstrahlung emission vanishes due to the divergence of the analytical DCS for small W, the restricted mean free path for radiative events with energy loss larger than a given nonzero value W_{cr},

$$\lambda^{-1}_{rad}(E;W_{cr}) = N \int_{W_{cr}}^E \frac{d\sigma_{rad}}{dW}\, dW, \tag{19}$$

is finite. The radiative stopping power

$$S_{rad}(E) = N \int_0^E W \frac{d\sigma_{rad}}{dW}\, dW \tag{20}$$

and the energy straggling parameter

$$\Omega^2_{\rm rad}(E) = N \int_0^E W^2 \frac{{\rm d}\sigma_{\rm rad}}{{\rm d}W}\, {\rm d}W \qquad (21)$$

are both finite. Radiative events can be simulated by means of mixed procedures (see Section 3.2), in which hard photon emission, with energy loss larger than $W_{\rm cr}$, is simulated in detail, whereas soft bremsstrahlung emission, with $W < W_{\rm cr}$, is accounted for by using the continuous slowing down approximation. Actually, the stopping effect of soft photon emission can be made negligibly small by using a suitably small value of $W_{\rm cr}$, i.e. detailed simulation is feasible in spite of the DCS divergence at $W = 0$. The present radiative DCS permits the random sampling of the energy loss W in hard events completely analytically (see Ref. [21]).

The radiative DCS given by Eq. (18) is quite accurate for electrons and positrons with kinetic energies larger than ~ 1 MeV; the stopping power computed from it agrees with the ICRU tables [30] within a few percent for much lower energies (generally down to some tens of keV, see Ref. [21]). For $E \leq 1$ MeV, $S_{\rm rad} \ll S_{\rm col}$, so that the present radiative DCSs are generally adequate for MC simulation of electron and positron transport at any energy. The accuracy of the simulation for energies below 1 MeV can be slightly improved by renormalizing our radiative DCS so as to reproduce the stopping power computed by more accurate methods [31,32].

In reality, the radiative DCS is a complicated function of the energy loss, the polar scattering angle of the projectile and the polar angle of the direction of emission of the photon [33] (spherical symmetry of the accelerating field is assumed). The angular distribution of the emitted photon is irrelevant here, since we are only interested in the simulation of electron and positron tracks. At high energies, where the radiative stopping power amounts to a significant fraction of the total stopping power, the mean number of high-energy photons emitted along an electron track is relatively small, and the effect of the angular deflections in these hard radiative events will be completely masked by the much stronger deflection due to multiple elastic scattering. On the other hand, the more probable emission of low-energy photons produces small angular deflections, which are assumed to be accounted for by the elastic scattering distribution. Therefore, we consider that the direction of movement of the projectile remains unaltered in radiative events.

2.4. Positron annihilation

Following Nelson et al. [12], we consider that positrons may annihilate in flight with electrons, assumed to be free and at rest, by emission of two photons. Electron binding effects, which enable one-photon annihilation (see, e.g., Ref. [34]), are neglected. The mean free path $\lambda_{\rm an}$ for two-photon annihilation is given by [12]

$$\lambda_{\rm an}^{-1} = NZ \frac{\pi r_{\rm e}^2}{(\gamma+1)(\gamma^2-1)} \times \left\{ (\gamma^2+4\gamma+1) \ln\left[\gamma + (\gamma^2-1)^{1/2}\right] - (3+\gamma)(\gamma^2-1)^{1/2} \right\}, \qquad (22)$$

where $r_{\rm e} = 2.8179\times10^{-15}$ m is the classical radius of the electron and $\gamma = 1 + E/mc^2$ is the total energy of the positron in units of its rest energy. Notice that, within this approximation, $\lambda_{\rm an}$ is a function only of γ and the electron density in the material.

2.5. Compound materials

When dealing with compounds, or mixtures, the habitual practice in MC simulation is to use the additivity rule, i.e. the molecular DCS is *approximated* as the sum of the corresponding DCSs of all the atoms in the molecule. Let us consider the case of a compound X_aY_b, whose molecules consist of a atoms of the element X and b atoms of the element Y. The number of electrons per molecule is $Z_{\rm M} = aZ(X) + bZ(Y)$ and the molecular weight is $A_{\rm M} = aA_{\rm w}(X) + bA_{\rm w}(Y)$, where $Z(X)$ and $A_{\rm w}(X)$ stand for the atomic number and atomic weight of element X. The number of molecules per unit volume is $N_{\rm M} = N_{\rm A}\rho/A_{\rm M}$.

The W2D model DCS for elastic scattering, see Eq. (6), is obtained from the mean free path and the first and second transport mean free paths *in the compound*. These can be calculated either from the atomic DCSs by means of the additivity rule or, more accurately, from the molecular DCS, which can be obtained as the squared modulus of the global scattering amplitude given by the coherent superposition of the waves scattered by the different atoms in the molecule [35]. In any case, elastic scattering in compounds can be simulated by using essentially the same scheme as for elemental materials. The molecular DCS for inelastic collisions in compounds is also given by Eq. (14) since the oscillators may pertain either to atoms or molecules. From the additivity rule, the mean excitation energy of the compound is

$$\ln I = Z_{\rm M}^{-1} \left[aZ(X) \ln I_X + bZ(Y) \ln I_Y \right], \qquad (23)$$

where I_X stands for the mean excitation energy of element X. For a discussion of the accuracy of this relation, see Ref. [30].

In the simulation of radiative events, we could use the molecular DCSs obtained from the additivity rule. The simulation of each radiative event would then consist of i) sampling the atom which participates in the interaction and ii) generating a random value of the energy loss from the corresponding atomic DCS. To save computer time, it is more convenient to consider an "equivalent" single element material of the same mass density ρ, atomic number $Z_{\rm eq}$ and atomic weight $A_{\rm eq}$ given by

$$Z_{\rm eq}A_{\rm M} = Z_{\rm M}A_{\rm eq} = aZ(X)A_{\rm w}(X) + bZ(Y)A_{\rm w}(Y), \qquad (24)$$

i.e. its atomic number (weight) is the mass-average (Z-average) of the atomic numbers (weights) of the constituent atoms. The number of "atoms" per unit volume in the equivalent material is $N_{eq} = N_A\rho/A_{eq}$. The radiative stopping power employed in the simulation is calculated from the additivity rule. Use of the equivalent material is made only to simulate radiative events; more precisely, these events are described by using the DCS of the element with the atomic number closest to Z_{eq}, renormalized so as to reproduce the radiative stopping power obtained from the additivity rule. Usually, this approximate procedure does not introduce appreciable errors and permits a considerable simplification of the calculation.

3. Mixed simulation algorithms

The single scattering model described in the previous section already allows the detailed Monte Carlo simulation of electron and positron transport in matter. Unfortunately, detailed simulation is only feasible for particles with initial kinetic energies up to ~500 keV, for which the number of events per track is reasonably small. Our aim here is to develop mixed simulation algorithms which permit the simulation of high-energy electron and positron transport much more quickly. In this kind of algorithms, hard events are simulated in detail, whereas the effect of the multiple soft interactions between each pair of consecutive hard events is simulated by means of suitable multiple scattering approaches. To make the arguments more precise, let us introduce the cutoff values μ_S, W_{cc} and W_{cr}. Elastic collisions with angular deflection $\mu \leq \mu_S$, inelastic collisions with energy loss $W \leq W_{cc}$ and emission of bremsstrahlung photons with $W \leq W_{cr}$ will be considered as soft interactions. Actually, for a given scattering model, one can devise a continuous variety of mixed algorithms, which are characterized by the cutoff values. Usually, the larger the cutoffs, the faster the simulation. However, approximations in the multiple scattering theories employed to describe soft interactions may set upper limits on the possible cutoff values.

For the sake of simplicity, we discuss here electron transport in a single-element medium. Positron transport is described in a similar way. The extension of the simulation algorithm to compounds and mixtures is performed by using the rules given above.

3.1. Elastic scattering

The W2D model allows the formulation of mixed simulation algorithms in a closed analytical form (see Eqs. (39)–(55) in Ref. [22]). As discussed in Ref. [22], it is convenient to specify the mixed algorithm by means of the mean free path $\lambda_{el}^{(h)}$ between hard elastic events rather than by the cutoff deflection μ_S. A convenient recipe to set the mean free path between hard elastic events is

$$\lambda_{el}^{(h)} = \max\{\lambda_{el}, C_1\lambda_1\}, \tag{25}$$

where C_1 is a preselected small constant (less than 0.1). The average angular deflection, $1 - \langle\cos\theta\rangle$, in a track segment of length $\lambda_{el}^{(h)}$ then approximately equals C_1 (see Ref. [16]). The quantity $\lambda_{el}^{(h)}$ increases with increasing energies, so that hard events are more spaced out when the scattering is weaker. Moreover, soft collisions are discontinued, i.e. the simulation becomes purely detailed when $C_1\lambda_1 < \lambda_{el}$.

In reality, elastic scattering coexists with inelastic collisions and bremsstrahlung emission, so that the particle loses energy along its track. The distance travelled by the particle from a given position to the following hard elastic collision is sampled from the mean free path $\lambda_{el}^{(h)}$ evaluated *at the beginning* of the step (there is no other alternative in this respect, since the length to be travelled up to the next hard collision, and hence the energy to be lost before colliding, is not known in advance). This introduces a certain systematic error, since the kinetic energy, and hence the properties of the interaction with the medium, may change appreciably along a single step. To keep this error below a reasonable limit, the energy loss in each step should be much smaller than the kinetic energy E at the beginning of the step. The mean energy loss in a step is given by

$$\langle\Delta E\rangle = \lambda_{el}^{(h)} S(E), \tag{26}$$

where

$$S(E) = S_{col}(E) + S_{rad}(E) \tag{27}$$

is the total stopping power. Therefore, the average fractional energy loss in a step can be made less than a preselected small value C_2 by taking

$$\lambda_{el}^{(h)}(E) = \max\left\{\lambda_{el}(E), \min\left[C_1\lambda_1(E), C_2\frac{E}{S(E)}\right]\right\}. \tag{28}$$

The parameters C_1 and C_2, which are selected by the user, serve to control the computer time needed to simulate each track. Ideally, they should not have any influence on the *accuracy* of the simulation results. This can be made sure by simply limiting their maximum values. Our experience is that simulation results are generally stable under variations of C_1 and C_2 within the interval $(0, 0.1)$ (see below). It should be noted that these two parameters act on different energy ranges. This is illustrated in Fig. 1, where the lengths λ_{el}, λ_1 and E/S for electrons in gold are represented as functions of the kinetic energy. The mean free path $\lambda_{el}^{(h)}$ for hard elastic events, determined from the prescription (28) with $C_1 = C_2 = 0.05$ is also plotted. For low energies, $\lambda_{el}^{(h)} = \lambda_{el}$ and the simulation is purely detailed ($\mu_S = 0$). For intermediate energies, $\lambda_{el}^{(h)} = C_1\lambda_1$, whereas $\lambda_{el}^{(h)} = C_2E/S(E)$ in the high-energy domain. From Fig. 1 it is clear that varying the value of C_2 does not have any effect on the simulation of electron tracks with initial energies that are less than ~ 1 MeV.

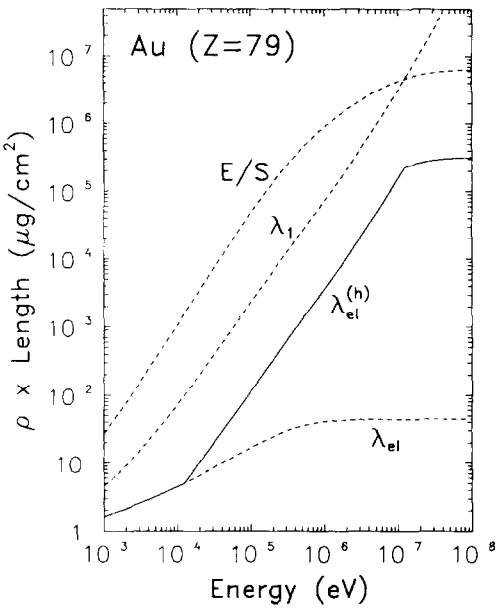

Fig. 1. Characteristic lengths λ_{el}, λ_1 and $E/S(E)$ (dashed curves) for electrons in Au. The mean free path between hard elastic events $\lambda_{el}^{(h)}$ (continuous curve) has been obtained from Eq. (28) with $C_1 = C_2 = 0.05$.

The global effect of the soft collisions experienced by the particle along a path segment of length t between two consecutive hard events is simulated as a single artificial elastic event, as described in Ref. [22]. The distance from the previous hard event to the artificial event is sampled uniformly in the interval $(0, t)$; this procedure gives the correct average spatial displacement at the end of the step and a consistent description of interface crossing (see Ref. [16]).

Computationally, it is faster to simulate a real elastic collision (i.e. to sample the random deflection μ from the W2D single scattering distribution) than to simulate an artificial elastic event. Therefore, when $\lambda_{el}^{(h)} < 2\lambda_{el}$, we will use strictly detailed simulation.

3.2. Energy loss

The high-energy codes currently available implement different approximate methods to simulate inelastic collisions and bremsstrahlung emission. Thus, ETRAN resorts to the multiple scattering theories of Landau [23] and Blunck and Leisegang [36], to obtain the energy loss distribution due to inelastic collisions after a given path length; the production of secondary electrons (delta rays) is simulated by means of the Møller DCS, which neglects binding effects. This approach accounts for the complete energy straggling, within the accuracy of the multiple scattering theory, but disregards the correlation between delta ray emission and energy loss in each track segment. Therefore, energetic delta rays can be generated in a track segment where the energy lost by the primary particle is smaller than the energy of the emitted delta rays. EGS4 uses a mixed procedure to simulate collision energy losses: hard inelastic collisions are simulated from Mott's DCS, thus neglecting binding effects, and soft inelastic collisions are described by means of the continuous slowing down approximation (CSDA), i.e. energy straggling due to soft inelastic collisions is ignored. As regards bremsstrahlung emission, EGS4 implements a mixed procedure in which hard radiative events are simulated in detail and use is made of the CSDA to simulate the effect of soft photon emission; ETRAN [9] uses strictly detailed simulation.

The use of the CSDA for soft stopping interactions (i.e. soft inelastic collisions and soft bremsstrahlung emission) is well justified when the energy straggling due to these interactions is negligible as happens when the cutoff energies W_{cc} and W_{cr} are both small, so that the fraction of the stopping power due to soft interactions is also small. To improve the description of energy straggling one should reduce the cutoff energies, but this enlarges the number of hard inelastic and radiative events to be simulated along each track and hence the simulation time. Our purpose is to go beyond the CSDA by introducing energy straggling in the description of soft stopping interactions. It is clear that, by proceeding in this way, we will be able to use larger values of the cutoff energies W_{cc} and W_{cr}, and hence speed up the simulation, without distorting the energy distributions.

The quantities that define our mixed simulation algorithm are the mean free paths $\lambda_{col}^{(h)}$ and $\lambda_{rad}^{(h)}$ for hard collisions and hard radiative events, and the stopping power S_s and the energy straggling parameter Ω_s^2 associated to soft stopping interactions. These quantities are given by

$$\lambda_{col}^{(h)}(E) = \left(N \int_{W_{cc}}^{E} \frac{d\sigma_{col}}{dW}\, dW \right)^{-1}, \tag{29}$$

$$\lambda_{rad}^{(h)}(E) = \left(N \int_{W_{cr}}^{E} \frac{d\sigma_{rad}}{dW}\, dW \right)^{-1}, \tag{30}$$

$$S_s(E) = N \int_0^{W_{cc}} W \frac{d\sigma_{col}}{dW}\, dW + N \int_0^{W_{cr}} W \frac{d\sigma_{rad}}{dW}\, dW \tag{31}$$

and

$$\Omega_s^2(E) = N \int_0^{W_{cc}} W^2 \frac{d\sigma_{col}}{dW}\, dW + N \int_0^{W_{cr}} W^2 \frac{d\sigma_{rad}}{dW}\, dW. \tag{32}$$

Let us consider that a particle, electron or positron, travels a step of length t between two consecutive events of any kind (i.e. artificial elastic events, hard elastic or inelastic collisions, hard bremsstrahlung emissions, and annihilation

in the case of positrons). Along this step, the particle is assumed to interact only through soft inelastic collisions and soft bremsstrahlung emission. We consider that the average energy loss in this path length, $S_s(E)t$, is much less than the initial energy E so that the DCSs can be assumed to stay essentially constant along the step. This can be guaranteed by simply taking a small enough value of the simulation parameter C_2, see Eq. (28) and Fig. 1, since the mean free path between consecutive hard events of any kind is shorter than the mean free path between hard elastic events. Let $G(\omega;t)$ denote the probability distribution function of the energy loss ω along the path length t; this distribution satisfies the following transport equation [23]

$$\frac{\partial G(\omega;t)}{\partial t} = N\int_0^\infty \left[G(\omega - W;t) - G(\omega;t)\right]\frac{d\sigma_s}{dW}\,dW \tag{33}$$

with the initial value $G(W;0) = \delta(W)$. Here, $d\sigma_s/dW$ stands for the DCS for soft stopping interactions, i.e.

$$\frac{d\sigma_s}{dW} = \frac{d\sigma_{col}}{dW}\Theta(W_{cc} - W) + \frac{d\sigma_{rad}}{dW}\Theta(W_{cr} - W). \tag{34}$$

A closed formal solution of the integral equation (33) may be obtained by considering its Fourier, or Laplace, transform with respect to ω (see e.g. Refs. [23,36]). For our purposes it is only necessary to know the first moments of the energy loss distribution after the path length t,

$$\langle\omega^n\rangle \equiv \int_0^\infty \omega^n G(\omega;t)\,d\omega. \tag{35}$$

From Eq. (33) it follows that

$$\begin{aligned}\frac{d}{dt}\langle\omega^n\rangle &= N\int_0^\infty d\omega\int_0^\infty dW\,\omega^n\left[G(\omega - W;t) - G(\omega;t)\right]\frac{d\sigma_s}{dW}\\ &= N\Big(\int_0^\infty d\omega'\int_0^\infty dW\,(\omega' + W)^n G(\omega';t)\frac{d\sigma_s}{dW}\\ &\quad - \langle\omega^n\rangle\int_0^\infty \frac{d\sigma_s}{dW}\,dW\Big)\\ &= \sum_{k=1}^{n}\frac{n!}{k!(n-k)!}\langle\omega^{n-k}\rangle N\int_0^\infty W^n\frac{d\sigma_s}{dW}\,dW,\end{aligned} \tag{36}$$

where use has been made of the fact that $d\sigma_s/dW$ vanishes when $W < 0$. In particular, we have

$$\frac{d}{dt}\langle\omega\rangle = N\int_0^\infty W\frac{d\sigma_s}{dW}\,dW = S_s, \tag{37}$$

$$\begin{aligned}\frac{d}{dt}\langle\omega^2\rangle &= 2\langle\omega\rangle N\int_0^\infty W\frac{d\sigma_s}{dW}\,dW + N\int_0^\infty W^2\frac{d\sigma_s}{dW}\,dW\\ &= 2\langle\omega\rangle S_s + \Omega_s^2\end{aligned} \tag{38}$$

and, hence

$$\langle\omega\rangle = S_s t, \tag{39}$$

$$\langle\omega^2\rangle = (S_s t)^2 + \Omega_s^2 t. \tag{40}$$

The variance of the energy loss distribution is

$$\mathrm{var}(\omega) = \langle\omega^2\rangle - \langle\omega\rangle^2 = \Omega_s^2 t, \tag{41}$$

i.e. the energy straggling parameter Ω_s^2 equals the variance increase per unit path length.

The key point in our argument is that soft interactions involve only comparatively small energy losses. If the number of soft interactions along the path length t is statistically sufficient, it follows from the central limit theorem that the energy loss distribution is Gaussian with mean $S_s t$ and variance $\Omega_s^2 t$, i.e.

$$G(\omega;t) \simeq \frac{1}{\left(2\pi\Omega_s^2(E)t\right)^{1/2}}\exp\left[-\frac{(\omega - S_s(E)t)^2}{2\Omega_s^2(E)t}\right]. \tag{42}$$

There is a close similarity between the present problem and that of the energy loss distribution of a heavy charged particle. In the latter case, owing to the large mass difference between the projectile and the target electrons, only fractionally small energy losses are kinematically allowed and, as a consequence, the observed energy loss distributions are nearly Gaussian. In the case of electrons, however, a large fraction of the kinetic energy of the projectile may be transferred in a single collision; a Gaussian energy loss distribution is obtained only when hard energy-loss events are switched off. A related discussion is given in Ref. [37].

The Gaussian energy loss distribution given by Eq. (42) is accurate only if i) the average energy loss $S_s(E)t$ is much smaller than E (so that the DCS $d\sigma_s/dW$ is nearly constant along the step) and ii) its standard deviation $[\Omega_s^2(E)t]^{1/2}$ is much smaller than its mean $S_s(E)t$ (otherwise there would be a non-zero probability of negative energy losses), i.e.

$$\left[\Omega_s^2(E)t\right]^{1/2} \ll S_s(E)t \ll E. \tag{43}$$

Requirement i) again implies that the cutoff energies W_{cc} and W_{cr} for delta ray production and photon emission have to be relatively small. The second requirement holds for path lengths larger than $t_{crit} = \Omega_s^2/S_s^2$.

Now, we address ourselves to the problem of simulating the energy losses due to soft stopping interactions. The distribution (42) gives the desired result when conditions (43) are satisfied. In fact, the use of a Gaussian distribution to simulate the effect of soft stopping interactions was previously proposed by Andreo and Brahme [20]. Unfortunately, the step lengths found in our simulations are frequently too short for conditions (43) to hold (i.e. t is usually less than $t_{\rm crit}$). To get over this problem, we will replace the actual energy loss distribution $G(\omega;t)$ by a simpler "equivalent" distribution $G_{\rm a}(\omega;t)$ with the same mean and variance, given by Eqs. (39) and (41). Other details of the adopted distribution have no effect on the simulation results, provided that the number of steps along each track is statistically sufficient (say, larger than ~ 20). The energy loss ω due to soft stopping interactions along a step of length t may take arbitrary values from 0 to E, with mean $\langle\omega\rangle$ ($\ll E$) and variance $\mathrm{var}(\omega)$ given by Eqs. (39) and (41). In the present simulations, ω is sampled from the distribution

$$G_{\rm a}(\omega;t) = b\delta(\omega) + (1-b)\frac{1}{\omega_2-\omega_1}\Theta(\omega-\omega_1)\,\Theta(\omega_2-\omega) \tag{44}$$

with

$$b = 0, \qquad \omega_1 = \langle\omega\rangle - [3\,\mathrm{var}(\omega)]^{1/2},$$
$$\omega_2 = \langle\omega\rangle + [3\,\mathrm{var}(\omega)]^{1/2}, \quad \text{if } \langle\omega\rangle^2 > 3\,\mathrm{var}(\omega) \tag{45}$$

and

$$b = \frac{3\mathrm{var}(\omega)-\langle\omega\rangle^2}{3\mathrm{var}(\omega)+3\langle\omega\rangle^2}, \qquad \omega_1 = 0,$$
$$\omega_2 = \frac{3\mathrm{var}(\omega)+3\langle\omega\rangle^2}{2\langle\omega\rangle}, \quad \text{if } \langle\omega\rangle^2 \le 3\mathrm{var}(\omega). \tag{46}$$

This distribution has the required mean and variance and the maximum energy loss, ω_2, is usually much less than E. Energy losses larger than E might be generated only when the step length has a value of the order of the Bethe range, and this is extremely unlikely.

It is worth noticing that, after a moderately large number of steps, this simple simulation scheme effectively yields an energy loss distribution due to soft stopping interactions that is nearly Gaussian with correct first and second moments. Further improvements of the distribution of soft energy losses would require the consideration of higher order moments of the single scattering DCS given by Eq. (34).

3.3. Scattering by atomic electrons

Most of the existing high-energy simulation codes have difficulties in accounting for the angular deflections of the projectile due to inelastic collisions (see e.g. Ref. [9]). The cross section differential in the scattering angle can be calculated approximately in terms of the incoherent scattering function [35]. This was the approach followed by Fano [38] to introduce electron scattering effects in the Molière theory. However, the DCS calculated in this way includes the totality of excitations and, hence, it is not adequate for mixed simulations, where scattering due to hard collisions is explicitly simulated. Moreover, the calculation of the DCS from the incoherent scattering function involves an average over excitation energies that cannot be performed exactly; instead, an effective minimum momentum transfer is introduced, which must be estimated empirically. This may cause inconsistencies for low energy projectiles.

A more consistent approach is obtained by simply computing the restricted angular DCS, for soft collisions with $W < W_{\rm cc}$, from our inelastic scattering model as follows. The (unnormalized) distribution function of Q in distant collisions with the i-th oscillator is (Eq. (30) in Ref. [21])

$$P_{\rm di}(Q) = \frac{1}{Q(1+Q/2mc^2)}, \qquad Q_- < Q < W_i. \tag{47}$$

The recoil energy Q and the angular deflection $\mu = (1-\cos\theta)/2$ are related through (see Eq. (11))

$$Q(Q+2mc^2) = 4cp\,cp_1\mu + (cp-cp_1)^2, \tag{48}$$

where p_1 is the momentum of the projectile after the collision,

$$(cp_1)^2 = (E-W_i)(E-W_i+2mc^2). \tag{49}$$

The probability distribution of the angular deflection in distant collisions can then be written as

$$P_{\rm di}(\mu) = P_{\rm di}(Q)\frac{{\rm d}Q}{{\rm d}\mu} = \frac{2mc^2}{4cp\,cp_1\mu+(cp-cp_1)^2}\frac{4cp\,cp_1}{2(Q+mc^2)}. \tag{50}$$

Considering that $Q \ll mc^2$ for the majority of soft distant collisions, the normalized distribution of μ in these collisions is

$$P_{\rm di}(\mu) = \left[\ln\left(\frac{4cp\,cp_1\mu_1+(cp-cp_1)^2}{(cp-cp_1)^2}\right)\right]^{-1} \times \frac{4cp\,cp_1}{4cp\,cp_1\mu+(cp-cp_1)^2}, \quad 0<\mu<\mu_1 \tag{51}$$

with

$$\mu_1 = \mu(Q=W_i) = \frac{W_i(W_i+2mc^2)-(cp-cp_1)^2}{4cp\,cp_1}. \tag{52}$$

On the other hand, the DCS per unit oscillator strength for soft ($W < W_{\rm cc}$) close collisions with the i-th oscillator is approximately given by the Rutherford formula

$$\frac{{\rm d}\sigma_{\rm ci}}{{\rm d}\mu} \simeq \frac{\pi e^4}{(p\beta c)^2}\frac{1}{\mu^2}, \qquad \mu_1 < \mu < \mu_2, \tag{53}$$

where e is the electron charge, βc is the speed of the projectile and

$$\mu_2 = \mu(Q = W_{cc}) = \frac{W_{cc}(W_{cc} + 2mc^2) - (cp - cp_2)^2}{4cp\, cp_2} \tag{54}$$

with

$$(cp_2)^2 = (E - W_{cc})(E - W_{cc} + 2mc^2). \tag{55}$$

Actually, close collisions should be described by the Møller (or Bhabha) DCS (see Ref. [21]); the use of the Rutherford DCS, which disregards exchange effects, facilitates the calculations considerably with a negligible loss of accuracy. Hence, the angular DCS for soft collisions is

$$\frac{d\sigma_{inel}^{(s)}}{d\mu} = \sum f_i \left[\sigma_{di} P_{di}(\mu) + \frac{d\sigma_{ci}}{d\mu}\right], \tag{56}$$

where σ_{di} is the total cross section per unit oscillator strength for distant collisions with the i-th oscillator (which can be evaluated analytically from Eq. (29) in Ref. [21]) and the summation extends over the oscillators with resonance energy less than W_{cc}.

The mean free path and the first and second transport mean free paths for soft inelastic scattering are given by

$$\left[\lambda^{-1}\right]_{inel}^{(s)} = N \int_0^{\mu_2} \frac{d\sigma_{inel}^{(s)}}{d\mu}\, d\mu, \tag{57}$$

$$\left[\lambda_1^{-1}\right]_{inel}^{(s)} = N \int_0^{\mu_2} 2\mu \frac{d\sigma_{inel}^{(s)}}{d\mu}\, d\mu \tag{58}$$

and

$$\left[\lambda_2^{-1}\right]_{inel}^{(s)} = N \int_0^{\mu_2} 6(\mu - \mu^2) \frac{d\sigma_{inel}^{(s)}}{d\mu}\, d\mu. \tag{59}$$

With the DCS given by Eq. (56), these quantities can be calculated analytically. The mean free path obtained from Eq. (57) practically coincides with the value obtained by integrating the "exact" energy loss DCS, Eq. (14); this validates the approximations introduced in deriving the angular DCS given in Eq. (56).

As mentioned above, the W2D model can be applied to any elastic scattering law. In particular, it can be used to describe the combined effect of pure elastic scattering and soft electronic scattering. This is accomplished by simply determining the parameters of the W2D model (see Eq. (7)) from the values of the mean free path and transport mean free paths of the combined process, instead of those of pure elastic scattering. The quantities that specify the combined scattering process are

$$\left[\lambda_{el}^{-1}\right]_{comb} = \lambda_{el}^{-1} + \left[\lambda^{-1}\right]_{inel}^{(s)}, \tag{60}$$

$$\left[\lambda_1^{-1}\right]_{comb} = \lambda_1^{-1} + \left[\lambda_1^{-1}\right]_{inel}^{(s)} \tag{61}$$

and

$$\left[\lambda_2^{-1}\right]_{comb} = \lambda_2^{-1} + \left[\lambda_2^{-1}\right]_{inel}^{(s)}. \tag{62}$$

4. Generation of random tracks

The history of each electron or positron history consists of a chronological succession of events. These can be either hard events, artificial elastic events or other relevant stages of the particle history (such as its initial state, the crossing of an interface or the effective absorption after slowing down). The trajectory of the particle between a pair of successive events is a straight segment, which will be referred to as a step.

Interactions qualified as hard events are hard elastic collisions ("el"), hard inelastic collisions ("col"), hard bremsstrahlung photon emission ("rad"), and positron annihilation ("an") when dealing with positrons. The simulation of hard events is performed in a detailed way by using the DCSs described in Section 2. The mean free path between consecutive hard events is given by

$$\frac{1}{\lambda^{(h)}} = \frac{1}{\lambda_{el}^{(h)}} + \frac{1}{\lambda_{col}^{(h)}} + \frac{1}{\lambda_{rad}^{(h)}} + \frac{1}{\lambda_{an}}. \tag{63}$$

The probability distribution function of the step length t between two successive hard events is

$$p(t) = \frac{1}{\lambda^{(h)}} \exp\left(-t/\lambda^{(h)}\right). \tag{64}$$

In each hard event, one and only one interaction (i = "el", "col", "rad" or "an") occurs with probability

$$p_i = \lambda^{(h)}/\lambda_i^{(h)}. \tag{65}$$

The combined effect of all (usually many) soft elastic collisions that occur between a pair of successive hard events separated a distance t is simulated as described in Ref. [22], i.e. as a single artificial elastic event in which the particle changes its direction of movement according to a probability distribution function $F_a(\theta; t)$ with the appropriate first and second moments. Other details of the $F_a(\theta; t)$ distribution are irrelevant when the number of hard events per track is larger than ~ 20. When mixed simulation of elastic scattering is effective, there is an artificial elastic event between each pair of successive hard events or, in other words, each step starts or ends with an artificial elastic event. Of course, the simulation of artificial elastic events is discontinued when the simulation becomes purely detailed (i.e., when $\lambda_{el}^{(h)} = 2\lambda_{el}$, cf. Section 3.1).

Owing to soft stopping interactions, when the particle travels a step of length t it loses an energy ω according to the probability distribution function $G_a(\omega; t)$, Eq. (44). In spatial dose calculations, this energy loss is considered to be locally deposited at a random point, which is sampled

uniformly along the step. This procedure yields dose distributions identical to those obtained by assuming that the energy loss is deposited at a constant rate along the step, but it is computationally simpler.

The simulation code PENELOPE generates random tracks by essentially following the scheme described in Ref. [22] for elastic scattering. Only slight modifications are needed to account for the energy loss along a track. The "state" of the particle immediately after an event is defined by its energy E, position coordinates $\boldsymbol{r}$ and direction cosines of its direction of movement $\hat{\boldsymbol{d}}$, as seen from the laboratory frame. It is assumed that particles are locally absorbed when their energy becomes smaller than a preselected value $E_{\rm abs}$; positrons are considered to annihilate after absorption. In the description of the algorithm we use the symbol $\leftarrow$ in expressions like "$a \leftarrow b$" to indicate that the value b replaces the value of a; ξ stands for a random number uniformly distributed in the interval (0,1). The practical generation of random electron and positron tracks in arbitrary material structures, which may consist of several homogeneous regions of different compositions separated by well-defined surfaces (interfaces), proceeds as follows;

(i) Set the initial kinetic energy E, position $\boldsymbol{r}$ and direction of movement $\hat{\boldsymbol{d}}$ of the primary particle.

(ii) Sample the distance t to be travelled up to the following hard event from the distribution given by Eq. (64). This is done by using the well-known sampling formula

$$t = -\lambda^{(\rm h)} \ln \xi. \tag{66}$$

(iii) Generate the length $\tau = t\xi$ of the step to the next artificial elastic event. Let the particle advance this distance in the direction $\hat{\boldsymbol{d}}$: $\boldsymbol{r} \leftarrow \boldsymbol{r} + \tau\hat{\boldsymbol{d}}$.

(iv) If the track has crossed an interface:
Stop it at the crossing point (i.e. redefine $\boldsymbol{r}$ as equal to the position of this point and set τ equal to the travelled distance).
Sample the energy loss ω due to soft stopping interactions along this step from the distribution $G_{\rm a}(\omega;\tau)$ and reduce the kinetic energy: $E \leftarrow E - \omega$.
Go to (ii) to continue the simulation in the new material, or go to (xii) if $E < E_{\rm abs}$ or the new material is the outer vacuum.

(v) Sample the energy loss ω due to soft stopping interactions along the step τ from the distribution $G_{\rm a}(\omega;\tau)$ and reduce the kinetic energy: $E \leftarrow E - \omega$.
Go to (xii) if $E < E_{\rm abs}$.

(vi) Simulate the artificial elastic event:
Sample the polar angular deflection θ from the distribution $F_{\rm a}(\theta;t)$. Sample the azimuthal scattering angle as $\phi = 2\pi\xi$. Perform a rotation $R(\theta,\phi)$ of the vector $\hat{\boldsymbol{d}}$ according to the sampled polar and azimuthal angular deflections (as described, e.g. in Refs. [14] and [39]) to obtain the new direction: $\hat{\boldsymbol{d}} \leftarrow R(\theta,\phi)\hat{\boldsymbol{d}}$.

(vii) $\tau \leftarrow t - \tau$.

(viii) Let the particle advance the distance τ in the direction $\hat{\boldsymbol{d}}$: $\boldsymbol{r} \leftarrow \boldsymbol{r} + \tau\hat{\boldsymbol{d}}$.

(ix) Do as in (iv).

(x) Do as in (v).

(xi) Simulate the hard event:
Sample the kind of interaction according to the point probabilities given by Eq. (65). Sample the polar scattering angle θ and the energy loss W from the corresponding DCS. Generate the azimuthal scattering angle as $\phi = 2\pi\xi$. Perform a rotation $R(\theta,\phi)$ of the vector $\hat{\boldsymbol{d}}$ to obtain the new direction: $\hat{\boldsymbol{d}} \leftarrow R(\theta,\phi)\hat{\boldsymbol{d}}$.
If, as a result of the interaction, a secondary electron (delta ray) is emitted in a direction $\hat{\boldsymbol{d}}_{\rm s}$, with energy $E_{\rm s} > E_{\rm abs}$, store its initial state ($E_{\rm s}$, $\boldsymbol{r}$, $\hat{\boldsymbol{d}}_{\rm s}$).
Reduce the kinetic energy of the particle: $E \leftarrow E - W$.
Go to (ii) if $E > E_{\rm abs}$.

(xii) Simulate the tracks of the secondary electrons produced by the primary particle (or by other secondaries previously followed) before starting a new primary track.

When the simulation of elastic scattering is purely detailed (i.e. when $\lambda_{\rm el}^{(\rm h)} = \lambda_{\rm el}$), the algorithm must be modified by skipping steps (vi) to (x) and setting $\tau = t$ in step (iii).

In order to simplify the calculations, the parameters of the multiple scattering distributions $F_{\rm a}(\theta;t)$ and $G_{\rm a}(\omega;\tau)$ are evaluated for the kinetic energy immediately after each hard event and are assumed to stay constant along the track length t between a pair of successive hard events (i.e. the effect of the energy loss due to soft stopping interactions on these distributions is disregarded). This approximation does not have any practical effect on the simulation results as long as the average fractional energy loss due to soft stopping interactions between successive hard events is small. This is made sure by simply using a value of the constant C_2 in Eq. (28) that is not too large.

As regards elastic scattering, it was shown in Ref. [22] that the present mixed algorithm gives a consistent description of spatial displacements and interface crossing. It is evident that this assertion remains valid when energy losses are included. We would like to emphasize that condensed algorithms find special difficulties in properly handling tracks in the vicinity of interfaces. In particular, they require the evaluation of the distance from each event to the nearest interface. PENELOPE is computationally much simpler since it only requires checking whether the track has crossed an interface.

Simulation with PENELOPE is controlled by the constants C_1 and C_2 and the cutoff energies $W_{\rm cc}$ and $W_{\rm cr}$. Hereafter, these four quantities will be referred to as simulation parameters. Essentially, the value of the mean free path $\lambda_{\rm el}^{(\rm h)}$ between hard elastic events is determined by the parameter C_1 (see Eq. (28)). As discussed by Baró et al. [22], this parameter should be small enough to ensure reliable simulation results. In the simulations we have used values of C_1 from 0 (detailed simulation) up to 0.1. The simulation parameter C_2 determines the maximum average fractional

energy loss between consecutive hard elastic events and is only effective at high energies (see Section 3.1). The cutoff energies W_{cc} and W_{cr} chiefly influence the simulated energy distributions. The simulation speeds up by using larger cutoff energies, but if these are too large the simulated energy distributions may be somewhat distorted. In practice, simulated energy distributions are found to be insensitive to the adopted values of W_{cc} and W_{cr} when these are less than the bin width used to tally the energy distributions. Thus, the desired energy resolution determines the maximum allowed cutoff energies.

The reliability of the whole simulation scheme rests on a single condition: the number of hard events of any kind per primary track must be "statistically sufficient", i.e. larger than ~ 20. When this condition is satisfied, we expect to obtain correct simulation results whatever the values of the adopted simulation parameters. In principle, we should use the largest values of the parameters that are compatible with the particular conditions of each experiment; these can be estimated from a few previous short trial simulations. We could also avoid any previous analysis by simply using "safe" values of the simulation parameters (e.g. $C_1 = 0.001$, $C_2 = 0.01$, $W_{cc} = W_{cr} = 0.01E_0$), at the expense of wasting some computer time.

5. Simulation results

We will limit our considerations to experiments in which a parallel electron or positron beam impinges normally on the surface of a homogeneous foil. Our simulation code gives the following information:

(i) Transmitted, backscattered and absorbed fractions, η_t, η_b and η_a respectively.

(ii) Energy distributions of transmitted and backscattered particles, $p_t(E)$ and $p_b(E)$, defined in such a way that $p_{t,b}(E)\,dE$ is the probability that an incident particle is transmitted, backscattered with energy in the interval $(E, E+dE)$. Thus, the integrals of these distributions equal the transmitted and backscattered fractions respectively.

(iii) Angular distributions of transmitted and backscattered particles, $p_t(\theta)$ and $p_b(\theta)$, where θ is the polar angle of the exit direction relative to the normal of the foil surface. $p_t(\theta)\,d\Omega$ is defined as the probability that an incident particle emerges from the foil in a direction within the solid angle element $d\Omega$ about the direction θ.

(iv) Mean energy of transmitted and backscattered primary particles, $\langle E\rangle_t$ and $\langle E\rangle_b$.

(v) Mean track length of transmitted, backscattered and absorbed primary particles within the foil, $\langle s\rangle_t$, $\langle s\rangle_b$ and $\langle s\rangle_a$.

(vi) Mean lateral displacement of transmitted and backscattered primary particles at the emergence point, $\langle (x^2+y^2)^{1/2}\rangle_t$ and $\langle (x^2+y^2)^{1/2}\rangle_b$.

(vii) Mean value of the polar direction cosine of the exit direction of transmitted and backscattered primary particles, $\langle \cos\theta\rangle_t$ and $\langle \cos\theta\rangle_b$.

5.1. Stability

An important feature of PENELOPE is its stability under variations of the simulation parameters. Table 1 sets out the simulation results for electrons with initial kinetic energy $E_0 = 1$ MeV impinging normally on a gold foil 0.1 mm thick; the absorption energy is $E_{abs} = 100$ keV. These results were obtained by using the indicated values of C_1 with fixed values of the other parameters, which were taken to be $C_2 = 0.1$ and $W_{cc} = W_{cr} = 10$ keV. The adopted value of C_2, which is somewhat too large for a realistic simulation of particles with higher energies, makes sure that the parameter C_1 is effective during the whole simulation (see Fig. 1), so that C_2 has no effect. The quoted simulation speeds (tracks/s) correspond to runs on a workstation HP Apollo 720; each simulation involved the generation of 10^5 random tracks. The statistical uncertainties (three standard deviations) given in the last column of Table 1 apply to the five sets of results. The simulation with $C_1 = 10^{-3}$ is purely detailed, i.e. $\lambda_{el}^{(h)} = \lambda_{el}$. It is seen that detailed simulation is about 40 times slower than mixed simulation with $C_1 = 0.1$. Apart from this fact, the simulation results are not significantly influenced by the value of C_1. It is not advisable to use larger values of the parameter C_1, if we want to keep the theoretical requirements that validate the mixed simulation scheme (see Ref. [22]).

The simulation parameter C_2 has an effect which is weaker than that of C_1. Indeed, when C_2 becomes effective (i.e. for energies which are high enough, see Fig. 1) its only action is to reduce the mean free path $\lambda_{el}^{(h)}$ for hard elastic events to a value which is less than $C_1\lambda_1$ (see Eq. (28)). Therefore, when C_2 comes into play the stability of the simulated angular (and spatial) distributions is reinforced. Our experience is that simulation results are practically insensitive to the adopted value of C_2 when it is less than ~ 0.05.

As mentioned above, simulated energy distributions are expected to be independent of the cutoff energies W_{cc} and W_{cr} when these are less than the bin width. This is illustrated in Fig. 2, where we compare simulated energy distributions of 1 MeV electrons transmitted through an aluminium foil 0.22 g/cm^2 thick obtained with different cutoff energies. Each histogram corresponds to 10^5 simulated tracks. The adopted values of the other simulation parameters are $C_1 = 0.05$ and $C_2 = 0.01$. For the sake of simplicity we have set $W_{cc} = W_{cr}$. Notice that the distributions simulated with $W_{cc} = 200$ eV and with $W_{cc} = 20$ keV (equal to the bin width) are identical, apart from small statistical fluctuations.

Naturally, maximum simulation speed is obtained by using cutoff energies W_{cc} and W_{cr} equal to the initial kinetic energy E_0 of the particle. However, this would effectively switch hard inelastic collisions and hard bremsstrahlung emission off and yield unphysical results. Even in this extreme case, the energy loss distribution after a step of length

Table 1
Simulation results for 1 MeV electrons impinging normally on a 0.1 mm thick gold foil. Additional details are given in the text

	C_1				
	10^{-3}	3×10^{-3}	10^{-2}	3×10^{-2}	10^{-1}
Tracks/s	0.620	1.08	2.73	7.95	25.4
η_t	21.11	21.07	21.45	21.20	21.60±0.39
η_b	46.18	46.09	45.96	46.12	45.74±0.47
η_a	33.63	33.80	33.65	33.73	33.66±0.45
$\langle E\rangle_t$ (keV)	592.6	592.2	591.6	591.6	593.7±3.5
$\langle E\rangle_b$ (keV)	727.9	725.8	725.4	725.9	725.7±2.7
$\langle s\rangle_t$ (μm)	211.7	211.8	212.0	212.5	211.1±1.6
$\langle s\rangle_b$ (μm)	134.6	135.4	135.5	135.3	135.5±1.3
$\langle s\rangle_a$ (μm)	360.9	361.9	361.8	361.3	362.5±1.5
$\langle\sqrt{x^2+y^2}\rangle_t$ (μm)	60.89	61.00	61.11	61.16	60.93±0.71
$\langle\sqrt{x^2+y^2}\rangle_b$ (μm)	51.43	51.64	51.77	51.71	51.75±0.46
$\langle\cos\theta\rangle_t$	0.723	0.724	0.720	0.722	0.719±0.004
$\langle\cos\theta\rangle_b$	−0.705	−0.705	−0.704	−0.704	−0.703±0.003

τ, $G_a(\omega;\tau)$, has correct first *and second* moments; the resulting energy distributions are therefore more realistic than those obtained with the strict CSDA, which ensures only the correctness of the mean energy loss. Actually, there is no point in using very large cutoff energies since the simulation speed tends to saturate for large cutoffs. This is a direct consequence of the fact that the most probable inelastic collisions and radiative events are those corresponding to low energy losses. On the other hand, a minimum of hard events per track (of the order of 20 or larger) is necessary to ensure the correctness of the high-energy-loss tail of the simulated energy distributions.

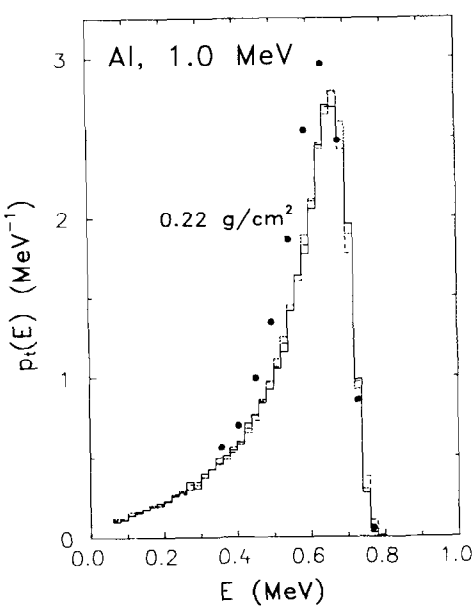

Fig. 2. Energy distributions of 1 MeV electrons transmitted through a 0.22 g/cm^2 thick aluminium foil. Histograms are simulation results obtained with different cutoff energies: W_{cc} = 200 eV (solid), W_{cc} = 20 keV (short-dashed) and W_{cc} = 40 keV (long-dashed). Dots are experimental data from Ref. [40].

5.2. Comparison with experiments

The ultimate test of the reliability of Monte Carlo simulation algorithms is provided by benchmark comparisons with experiments. A wealth of experimental data exists for electron beams impinging normally on foils of various materials, although data from different authors may differ considerably in some cases. Our aim here is to give a global view of the capabilities of the mixed algorithm implemented in PENELOPE rather than an exhaustive comparison with available experimental data. In order to ensure that effects related to bremsstrahlung photon transport are negligible, we consider either low-atomic number materials (in the case of high energies) or low energy particles. In all cases, the number of simulated primary tracks is of the order of 100 000.

Elastic scattering has the dominant effect on the angular distributions of transmitted electrons. In Fig. 3, simulated angular distributions of 15.7 MeV electrons transmitted through gold foils of two different thicknesses are compared with experimental data of Hanson et al. [41]. The agreement between simulation results and experiment is good, in spite of the fact that the distributions are very sharp. Comparison with the experimental data of Rester and Derrickson [40], see Fig. 4, reveals a similar agreement. From the analysis given in Ref. [22], it is concluded that the present simulation algorithm yields realistic angular distributions for much lower energies, down to $\sim$ 1 keV, where condensed simulation schemes are unsatisfactory [42].

Energy loss distributions of transmitted electrons are es-

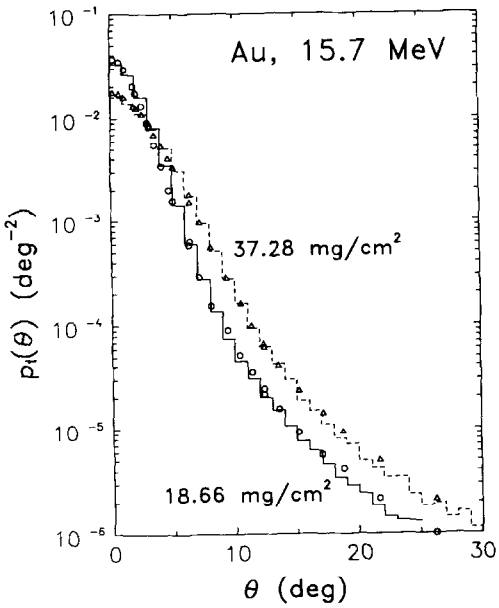

Fig. 3. Angular distributions of 15.7 MeV electrons transmitted through gold foils of the indicated thickness. Triangles and circles are experimental data from Ref. [41], scaled to match the simulation results (histograms) at $\theta \sim 5°$.

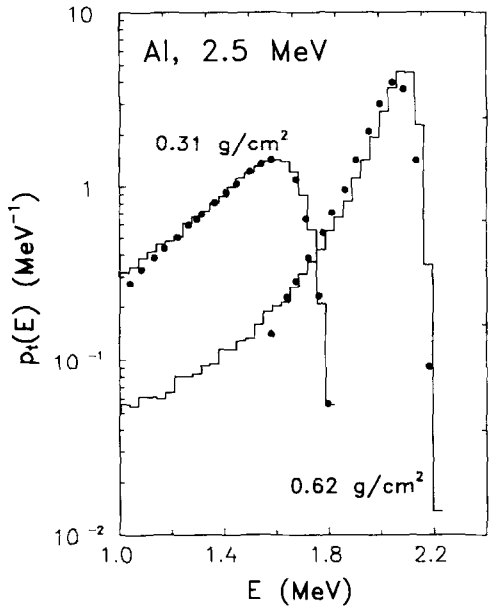

Fig. 5. Energy distributions of 2.5 MeV electrons transmitted through aluminium foils of the indicated thicknesses. Histograms represent simulation results. Dots are experimental data from Ref. [40].

sentially sensitive to inelastic scattering (low energies), and bremsstrahlung emission (high energies). Simulation results from PENELOPE compare well with experiments over a wide energy range, as exemplified in Figs. 2, 5 and 6. The experimental data in Figs. 2 and 5 are from Ref. [40], and have been shown to agree also with results from condensed simulation codes (see e.g. Ref. [9]). For energies as low as 20 keV (Fig. 6), our results agree reasonably with experiments and, even more closely with results obtained from detailed simulations using more realistic scattering models [44].

A quantity of importance in dosimetry is the depth dose distribution (= deposited energy per unit depth). Fig. 7 com-

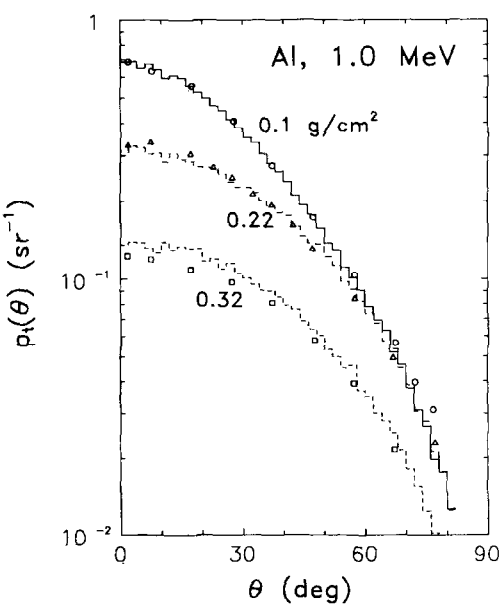

Fig. 4. Angular distributions of 1 MeV electrons transmitted through aluminium foils of the indicated thicknesses. Histograms are simulation results, special symbols represent experimental data from Ref. [40].

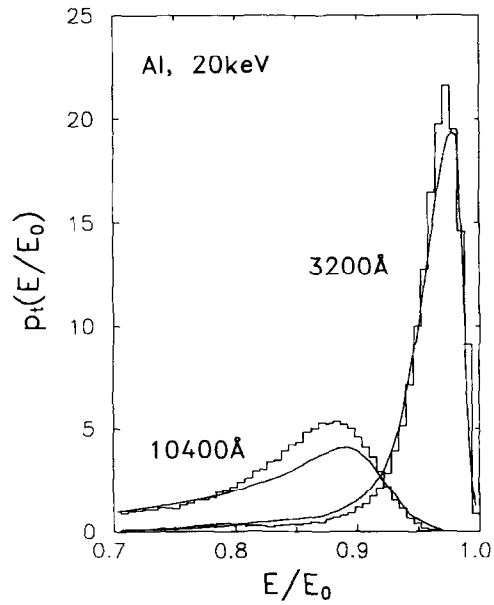

Fig. 6. Energy distributions of 20 keV electrons transmitted through aluminium foils of the indicated thicknesses. Simulation results are represented as histograms. Curves are results from experiments by Shimizu et al. [43].

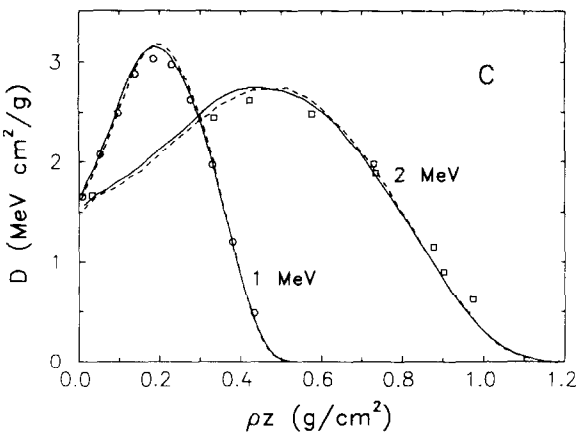

Fig. 7. Depth dose functions for 1 and 2 MeV electrons impinging normally on a thick carbon slab. The continuous curves represent simulation results from PENELOPE. Dashed lines are results generated with the ITS/TIGER code [45]. Circles and squares are experimental data quoted by Andreo et al. [45].

pares depth dose distributions of 1 and 2 MeV electrons in carbon obtained from PENELOPE with experimental data and simulation results calculated with the ITS/TIGER simulation code (a subset of the ETRAN system) by Andreo et al. [45]. The differences between the results from PENELOPE and ITS, which are seen to increase with increasing energies, are due to the transport of bremsstrahlung photons. Simulated depth dose distributions of electrons with energies from 15 to 50 keV and recently published experimental data from Werner et al. [46] are displayed in Fig. 8. Here, experimental data have been renormalized to delimit the same area as the experimental distributions. This comparison gives a clear demonstration of the reliability of PENELOPE's results for low energies.

The energy dependence of the backscattered fraction in

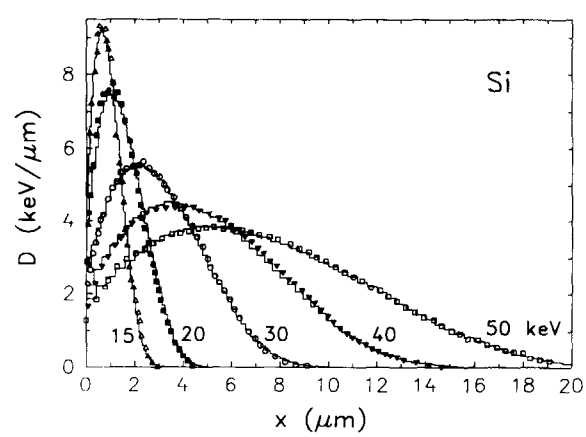

Fig. 8. Depth dose functions for electrons impinging normally on a thick silicon foil with the indicated energies. Histograms are simulation results. Symbols are experimental data from Ref. [46] (scaled as indicated in the text).

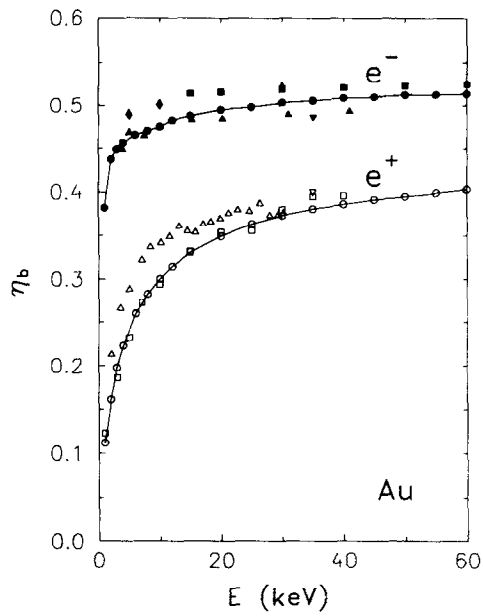

Fig. 9. Backscattered fractions of electrons (full symbols) and positrons (open symbols) impinging normally on thick gold foils, as functions of the kinetic energy. Simulation results are indicated by circles, joined by straight segments for visual aid. Other symbols represent experimental data from different authors. a) Electrons: squares, Ref. [47]; triangles, Ref. [48]; inverted triangles, Ref. [49]; and rhombi, Bishop, quoted in Ref. [47]. b) Positrons: triangles, Ref. [50]; inverted triangles, Ref. [49]; and squares, Ref. [51].

thick targets provides another global check of the reliability of the simulation for intermediate and low energies. In particular, the striking differences between electron and positron backscattering coefficients at low energies should be properly reproduced. PENELOPE yields realistic values of backscattering coefficients and gives electron-positron differences in excellent agreement with the most recent data available. This is illustrated in Fig. 9, which sets out simulated backscattering coefficients for electrons and positrons in gold, together with experimental data from different authors. Simulated backscattering fractions for positrons agree well with recent experimental data from Coleman et al. [51], which are claimed to be substantially more accurate than previously measured ones.

In conclusion, PENELOPE offers a reliable description of electron and positron transport in arbitrary materials and in a wide energy range. The algorithm is adequate for most practical purposes, only experimental arrangements involving high energy resolution and/or high angular resolution would require a more accurate treatment. With the mixed simulation method implemented in PENELOPE, the description of spatial displacements and interface crossing is more accurate, and simpler, than with the habitual condensed algorithms.

Acknowledgement

We are indebted to Dr. D. Liljequist for stimulating discussions and for critically reading the manuscript. This work has been partially supported by the Dirección General de Investigación Científica y Técnica (SPAIN) under contract no. PB92-0801-C02-01.

References

[1] Chr. Bargholtz, L. Holmberg, K. E. Johansson, D. Liljequist, P.-E. Tegnér and D. Vodjani, Phys. Rev. C 40 (1989) 1188.
[2] A. Spalek and O. Dragoun, J. Phys. G 19 (1993) 2071.
[3] L. Reimer, Electron Scanning Spectroscopy (Springer, Berlin, 1985).
[4] H.W. Werner and R.P.H. Garten, Rep. Prog. Phys. 47 (1984) 221.
[5] P.J. Schultz and K.G. Lynn, Rev. Mod. Phys. 60 (1988) 701.
[6] P. Andreo, Phys. Med. Biol. 36 (1991) 861.
[7] H.A. Bethe, M.E. Rose and L.P. Smith, Proc. Am. Philos. Soc. 78 (1938) 573.
[8] W.T. Scott, Rev. Mod. Phys. 35 (1963) 231.
[9] Monte Carlo Transport of Electrons and Photons, eds. T.W. Jenkins, W.R. Nelson and A. Rindi (Plenum, New York, 1988).
[10] A. Jablonski, Phys. Rev. 43 (1991) 7546.
[11] J.D. Martínez, R. Mayol and F. Salvat, J. Appl. Phys. 67 (1990) 2955.
[12] W.R. Nelson, H. Hirayama and D.W.O. Rogers, Stanford Linear Accelerator Center Report SLAC-265 (Stanford, 1985).
[13] R. Brun, F. Bruyant, M. Maire, A.C. McPherson and P. Zanarini, CERN Report DD/EE/84-1 (Geneva, 1986).
[14] M.J. Berger, in: Methods in Computational Physics, vol. 1, eds. B. Alder, S. Fernbach and M. Rotenberg (Academic Press, New York, 1963) p. 135.
[15] G. Molière, Z. Naturforsch. 3a (1948) 78.
[16] J.M. Fernández-Varea, R. Mayol, J. Baró and F. Salvat, Nucl. Instr. and Meth. B 73 (1993) 447.
[17] P. Andreo, J. Medin and A. F. Bielajew, Med. Phys. 20 (1993) 1315.
[18] A.F. Bielajew and D.W.O. Rogers, Nucl. Instr. and Meth. B 18 (1987) 165.
[19] L. Reimer and E.R. Krefting, Nat. Bur. Stand. (U.S.), Spec. Publ. 460 (US Government Printing Office, Washington DC, 1976) p. 45.
[20] P. Andreo and A. Brahme, Radiat. Res. 100 (1984) 16.
[21] F. Salvat and J.M. Fernández-Varea, Nucl. Instr. and Meth. B 63 (1992) 255.
[22] J. Baró, J. Sempau, J.M. Fernández-Varea and F. Salvat, Nucl. Instr. and Meth. B 84 (1994) 465.
[23] L. Landau, J. Phys. (Moscow) 8 (1944) 201.
[24] J. Baró, M. Roteta, J.M. Fernández-Varea and F. Salvat, Radiat. Phys. Chem. 44 (1994) 531.
[25] F. Salvat and R. Mayol, Comput. Phys. Commun. 74 (1993) 358.
[26] F. Salvat, J.D. Martínez, R. Mayol and J. Parellada, Phys. Rev. A 36 (1987) 467.
[27] J.M. Fernández-Varea, R. Mayol and F. Salvat, Nucl. Instr. and Meth. B 82 (1993) 39.
[28] E. Zeitler and H. Olsen, Phys. Rev. 136 (1964) A1546.
[29] C.M. Lederer and V.S. Shirley, Table of Isotopes, Appendix III (Wiley, New York, 1978).
[30] M.J. Berger and S.M. Seltzer, Nat. Bur. Stand. Rep. NBSIR 82-2550 (Washington, 1982). Also available as ICRU Report 37 (1984).
[31] S.M. Seltzer and M.J. Berger, Nucl. Instr. and Meth. B 12 (1985) 95.
[32] S.M. Seltzer and M.J. Berger, Atomic Data and Nuclear Data Tables 35 (1986) 345.
[33] H.W. Koch and J.W. Motz, Rev. Mod. Phys. 31 (1959) 920.
[34] W. Heitler, Quantum Theory of Radiation (Oxford Univ. Press, London, 1954) 3rd ed.
[35] N.F. Mott and H.S.W. Massey, The Theory of Atomic Collisions (Oxford Univ. Press, Oxford, 1965).
[36] O. Blunck and S. Leisegang, Z. Phys. 128 (1950) 500.
[37] E.J. Williams, Proc. Roy. Soc. London 125 (1929) 420.
[38] U. Fano, Phys. Rev. 93 (1954) 117.
[39] F. Salvat, J.D. Martínez, R. Mayol and J. Parellada, Comput. Phys. Commun. 42 (1986) 93.
[40] D.H. Rester and J.H. Derrickson, J. Appl. Phys. 42 (1971) 714
[41] A.O. Hanson, L.H. Lanzl, E.M. Lyman and M.B. Scott, Phys. Rev. 84 (1951) 634.
[42] C.T. Ballinger, D.E. Cullen, S.T. Perkins, J.A. Rathkopf, W.R. Martin and S.J. Wilderman, Nucl. Instr. and Meth. B 72 (1992) 19.
[43] R. Shimizu, Y. Kataoka, T. Ikuta, T. Koshikawa and H. Hashimoto, J. Phys. D 9 (1976) 101.
[44] J.M. Fernández-Varea, D. Liljequist and F. Salvat, to be published.
[45] P. Andreo, R. Ito and T. Tabata, Report RIAST-UOP-TR 1, Research Institute for Advanced Science and Technology, Univ. of Osaka Prefecture (1992). See also Atomic Data and Nuclear Data Tables 56 (1994) 105.
[46] U. Werner, F. Koch and G. Oelgart J. Phys. D 21 (1988) 116.
[47] G. Neubert and S. Rogaschewski, Phys. Stat. Sol. (a) 59 (1980) 35.
[48] H.-J. Hunger and L. Küchler, Phys. Stat. Sol. (a) 56, (1979) k45.
[49] G.R. Massoumi, N. Hozhabri, W.N. Lennard and P.J. Schultz, Phys. Rev. B 44 (1991) 3486.
[50] J. Mäkinen, S. Palko, J. Martikainen and P. Hautojärvi, J. Phys. Condens. Matter 4 (1992) L503.
[51] P.G. Coleman, L. Albrecht, K.O. Jensen and A.B. Walker, J. Phys.: Condens. Matter 4 (1992) 10311.